A Theoretical Study on the Structure of Poly((*R*)-3-hydroxybutanoic acid)

Yu-Xue Li[†] and Yun-Dong Wu*[,†,‡]

Institute of Theoretical and Computational Chemistry, State Key Laboratory of Molecular Dynamics and Stable Structures, College of Chemistry, Peking University, Beijing, China, and Department of Chemistry, The Hong Kong University of Science & Technology, Clear Water Bay, Kowloon, Hong Kong, China

Received: February 13, 2003

Conformational features of oligomers of 3-(*R*)-butanoic acid have been studied using quantum mechanics methods. Conformational search of Ac−$OCH(CH_3)$−CH_2−$COOCH_3$ indicates that the compound is quite flexible with several conformations similar in stability. Study of Ac−$[OCH(CH_3)-CH_2-CO]_nOCH_2CH_3$, $n = 1-8$, using a repeating unit approach for 2_1-helix, 3_1-helix, 4_1-helix, 5_1-helix, and pleated strand structure indicates that only the 3_1-helix has a cooperative effect and is also most stable. Crystal orbital calculations on the crystal packing energies of the 2_1-, 3_1-, and 4_1-helices have been performed. The 2_1-helix is found to have much stronger crystal packing stabilization than the 3_1- and 4_1-helices. This explains why the 2_1-helix is found in crystal structures of poly((*R*)-3-hydroxybutanoic acid) (PHB) despite the fact that the 3_1-helix is the most stable single helix. The stabilization of the 2_1-helix in the crystal structure is mainly from the dipole interaction between adjacent parallel helices but not from adjacent antiparallel helices. The study also provides useful information for the study of ion channel structures of PHB.

Introduction

The biopolymer poly((*R*)-3-hydroxybutanoic acid) (PHB) has attracted a lot of attention in recent years.[1] PHBs are synthesized by microorganisms as storage materials of high molecular weight (about 10^6 Da) under conditions of nutrient limitation.[1a] PHBs can serve as biodegradable plastics and have been used to replace conventional plastics in a variety of applications.[1c,1e,2] Short-chain PHBs have been found in cell membranes and serve as ion channels, together with polyphosphates (PPi).[3] In addition, Seebach and co-workers have found that synthetic short-chain PHBs can cause phospholipid membranes to become permeable for cations, such as Na, K, Rb, Ca, or Ba, both under voltage-gated and under concentration-driven conditions.[4]

The exact structure of ion channels consisting of PHB is still unknown.[3j] In stretched fibers and in lamellar crystals, PHBs are found to fold in a 2_1-helix structure.[5] In cyclic oligomers of HB, basic structural units for 2_1- and 3_1-helices and for pleated sheet structures have been revealed by Seebach and co-workers.[1b−d,6] These have led to the proposal of several models for PHB/PPi channels.[1b−c,3a,3f] In solution, NMR studies have shown that oligomeric hydroxybutanoic acid (OHB) backbone is quite flexible and there does not seem to be a significant preference for a particular conformation.[7] CD spectra of OHBs and FRET measurements of OHBs with double fluorescence-labeled OHBs containing 8, 16, and 32 HB units indicate, however, the possible existence of chiral secondary structures of these intermediate chains on the short time scale of UV/vis spectroscopy.[8] Such conformational features of OHBs are quite different from those of analogous β-peptides and oxapeptides, which display a strong tendency to form secondary structures in solution.[9]

While the conformational features of β-peptides and oxapeptides have been extensively investigated theoretically,[10,11] there have been relatively few theoretical studies on the conformational features of OHB or PHB. A recent molecular mechanics simulation study on OHB indicated the flexible backbone feature as observed by experiments.[12] To have a more detailed understanding of PHB structure, we have performed a theoretical study at ab initio level on several OHB models. Using a diester model, we carried out a conformational search to find energetically favorable conformers. Then several secondary structures of single-chain OHB were studied with a repeating unit method. It was found that in the gas phase, OHB in 2_1-helix is not stable compared with the 3_1-helix. Finally, crystal orbital calculations were carried out, which revealed that the 2_1-helix has a strong crystal packing stabilization. This provides an understanding why the 2_1-helix is found in crystal structures and stretched fibers. The results also provide useful information for understanding the structure of PHB ion channels.

Computational Methodology

To find the basic conformational features of PHB, we have carried out a conformational search on a diester model **1**. As shown in Figure 1, each HB unit has three rotatable single bonds, and each bond has three important conformations: gauche, −gauche, and anti. Instead of exploring the whole potential energy surface, only those $3^3 = 27$ important conformers were investigated. Their geometries were optimized with the B3LYP/6-311G* method[13] using the Gaussian 98 program.[14] Harmonic vibration frequency calculation with which thermal corrections were made was carried out for each structure. Solvent effect was also evaluated with the SCIPCM[15] calculations with $\epsilon = 33$ (methanol) and isodensity value of 0.0004 using the Gaussian 94 program.[16]

Five interesting secondary structures were constructed on the basis of the stable conformations of model **1**. The stabilities of these polymers were investigated using a repeating unit scheme.

* To whom correspondence should be addressed. E-mail: chydwu@chem.pku.edu.cn.
[†] Peking University.
[‡] The Hong Kong University of Science & Technology.

10.1021/jp0343741 CCC: $25.00
Published on Web 06/03/2003

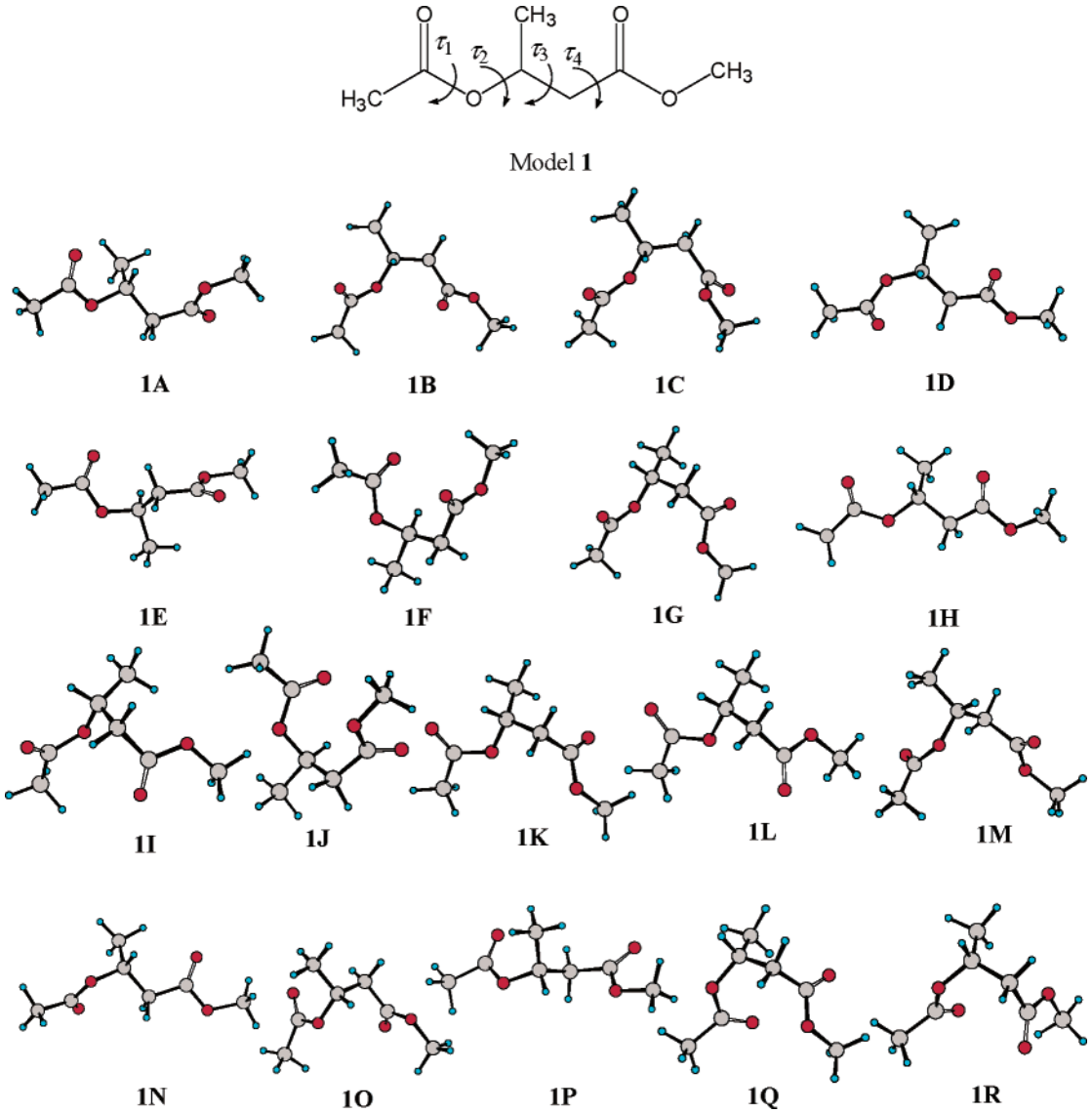

Figure 1. Diester model **1** and its 18 stable conformers optimized by the B3LYP/6-311G* method. The sequence of these structures is the same as the order of their free energies in the gas phase (Table 1).

The repeating units for the five structures were obtained by geometrical optimization with a hexaester model Ac−(CHMe−CH_2−CO)$_5$−OCH_2CH_3 (Figure 2). The six ester units in each secondary structure were constrained in the same geometry so that geometrical optimization gave the repeating unit (actually the average geometry), which was used to build oligomeric esters Ac−(CHMe−CH_2−CO)$_n$−OCH_2CH_3, $n = 1-8$. The energies of such built ester models were calculated with the B3LYP/6-311G* and MP2/6-311G* methods without further geometrical optimization. Such repeating unit approach method has been applied to the study of helical and sheet structures of α- and β-peptides.[10d−e,17]

To compare the crystal packing energies of 2_1-, 3_1-, and 4_1-helices, ab initio self-consistent-field crystal orbital (CO) calculations have been performed with the CRYSTAL98 program package[18] at the B3LYP/3-21G level. The shrinkage factor was set to 40, 10, and 5 for 1D, 2D, and 3D models, respectively. The 2_1-, 3_1-, and 4_1-helices of a hexaester model were studied. Full geometrical optimization results in imperfect 2_1-, 3_1-, and 4_1-helical structures. To get structures with prefect translational symmetries, the translationally equivalent methyl groups (the side chains in one side) of the hexaester model Ac−(CHMe−CH_2−CO)$_5$−OCH_2CH_3 were confined into a plane during the optimization using the B3LYP/6-311G* method with the Gaussian 98 program package. Thus a perfect helix can be preserved in the optimized structure. The middle part of the optimized hexaester was used as the repeating unit structure in the crystal orbital calculation. The 1D infinite single polymer models **2**, **8**, and **14** (Figure 3) were used as benchmarks for the calculation of crystal packing energy. The energy per HB unit (CH_2−CO−OCHMe) of the 1D model was used as the zero energy level, E_0. The crystal packing energy, E_p, is defined as follows:

$$E_p = \frac{E_{cell}}{n} - E_0$$

where E_{cell} is the energy per unit cell and n is the number of HB units per unit cell.

As for the 2_1-helix, the 3D crystal structure model (**7**) can be derived from experiment. But for the 3_1- and 4_1-helices, no crystal structure is available, and we have to derive their 3D crystal packing models on the basis of computational experiments. The structures were derived from some supposed rules and test calculations: (a) For helical polymers, the neighboring

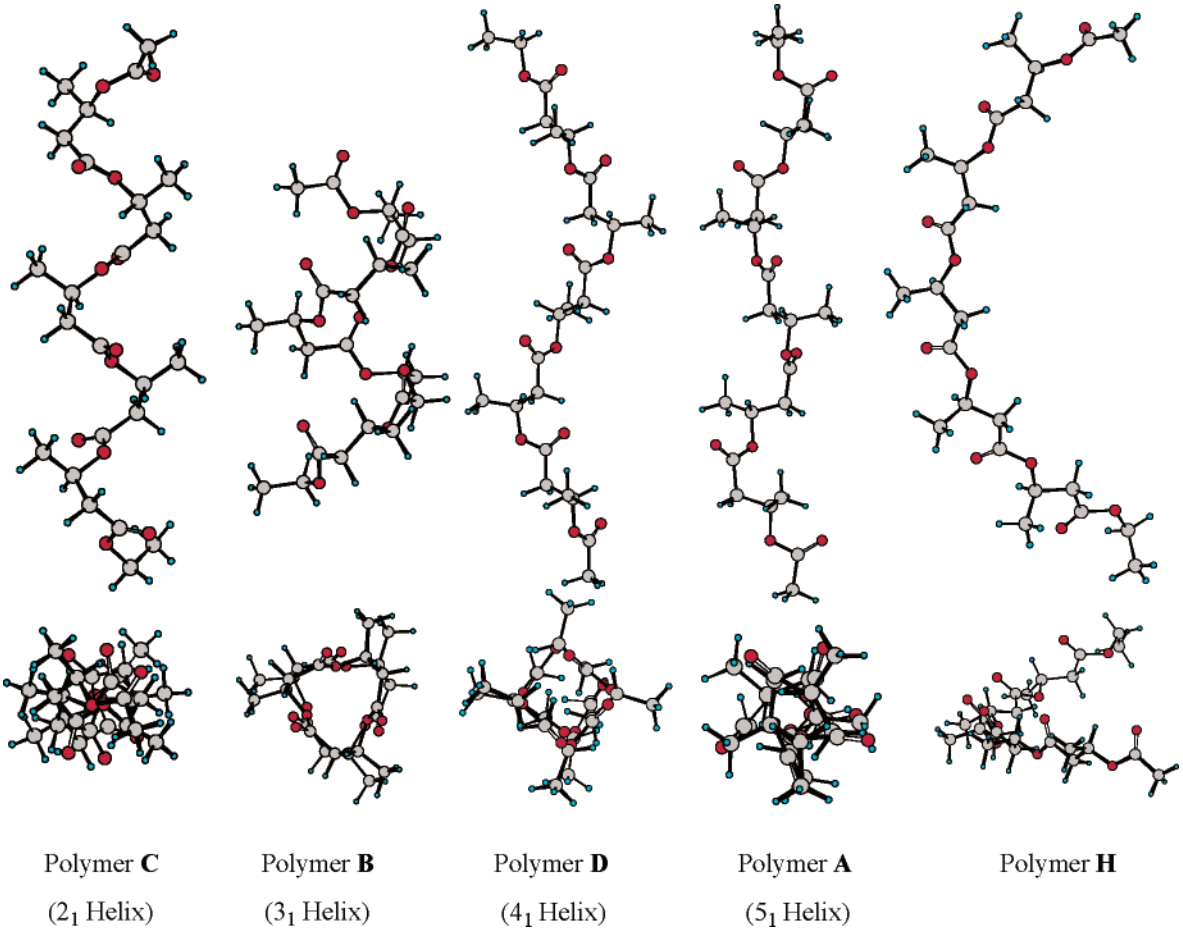

Figure 2. Structures of polymers **A**, **B**, **C**, **D**, and **H** optimized with a repeating unit approach using the B3LYP/6-311G* method.

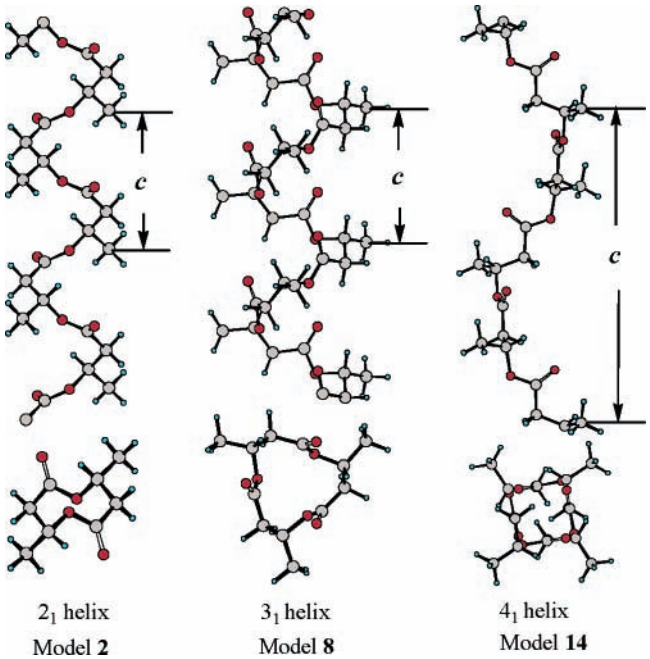

Figure 3. Single polymer models used in crystal orbital calculation. *c* is the translational distance along the polymer axis. These structures were optimized at the B3LYP/6-311G* level using a hexaester model in which the translationally equivalent methyl groups are confined into a plane during the optimization.

helices should be parallel or antiparallel; thus the backbone of neighboring helices are parallel and should match each other well in geometric space so that the two adjacent polymer chains can become closest. (b) Between two parallel or antiparallel neighboring helices, there should be no too close or too far atom pairs. In that case, only a few backbone-parallel orientations are favorable. (c) To obtain a good 3D structure, the packing pattern should be energetically favorable and have relatively high symmetry, which is important for deriving the most condensed packing. In the crystal structure of 2_1-helix, the polymer chains are like cuboids packing together and the methyl carbons and the carbonyl oxygen atoms define the sides of the cuboids. For the 3_1- and 4_1-helices, we treated them as triangular or cuboid prisms, and their sides are defined by the methyl carbon atoms. The possible 2_1-helix axis and C_2 axis are positioned so that the best match of the polymer chains can be obtained. There are parallel and antiparallel helix parings simultaneously in the 3D crystals because the long polymer chain must run many times across the crystal.[1c] A 3D crystal structure can be considered as being constructed by different kinds of 2D slabs, and the 2D slabs are composed of double polymer chains. A double polymer chain model can characterize a basic interaction type between polymer chains in the 3D structure. It is representative for the 3D crystal. To determine the most favorable 3D structures, we studied the possible packing patterns of two neighboring helices first. Antiparallel and parallel double chain models **3**, **4**, **9**, **10**, **15**, and **16** were used (Figures 4−6). In these models, the distance between two polymer chains was optimized using pointwise optimization method, that is, we calculated the energy while changing the interchain distance point by point (without geometrical optimization with each point), until change in energy is smaller than

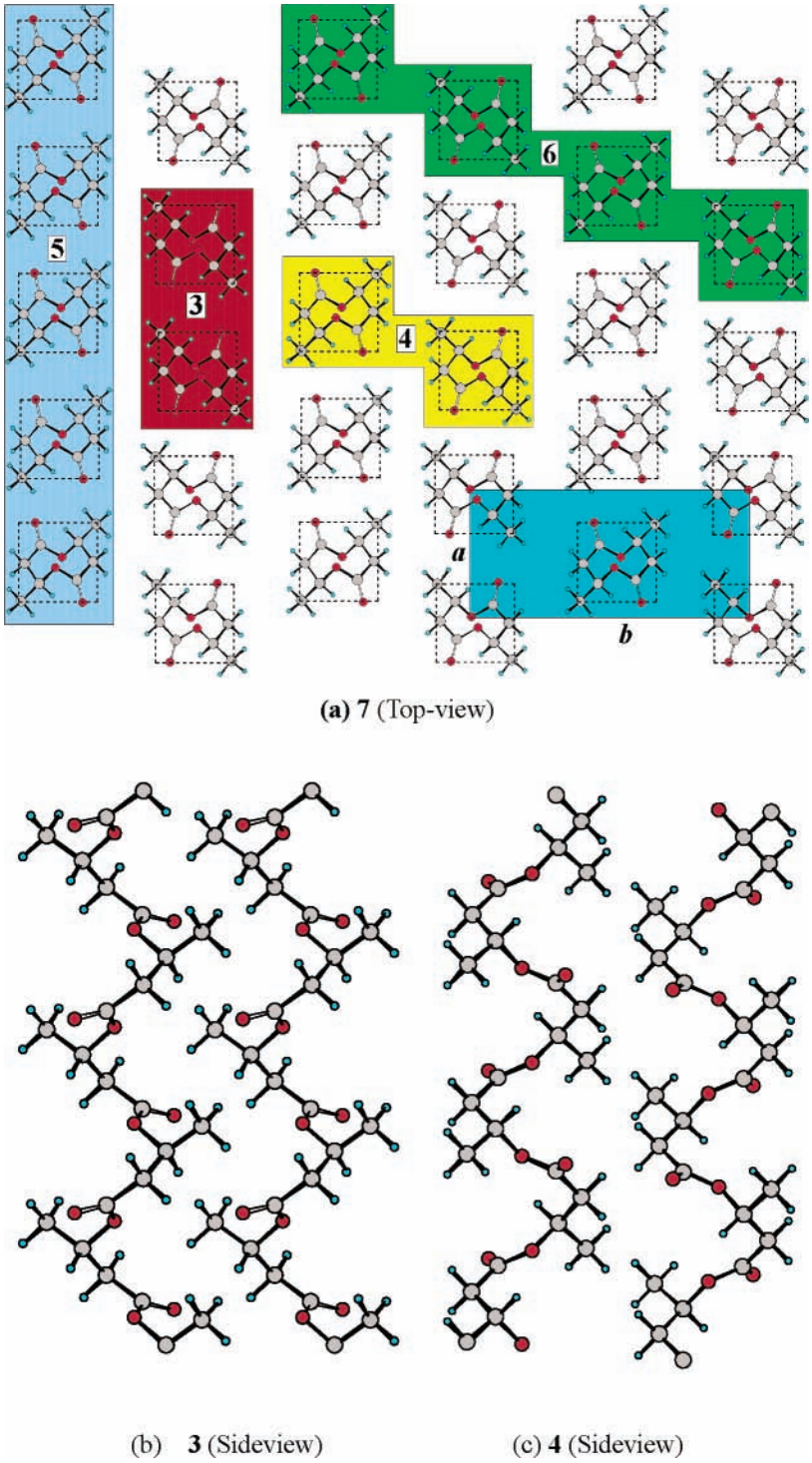

Figure 4. Top view (a) of 3D crystal model **7** constructed by 2_1-helix. All of the other models are part of the 3D model. Models **3** and **4** are parallel and antiparallel double helix; models **5** and **6** are parallel and antiparallel slabs. **a** and **b** are translational vectors. Panel b shows a side view of model **3** in which the carbonyl groups align head-to-tail. Panel c shows a side view of model **4**. The carbonyl groups are shoulder-to-shoulder.

0.01 kcal/mol. The optimized distances were then used as translational distances for 2D and 3D structures. The optimized double chain models were then used to construct 3D structures and infinite 2D slabs that represent a main interaction type in 3D crystal structure.

To testify whether these proposed models were the most favorable packing patterns, we did an exhaustive search using models **9** and **10**. For model **9**, we fixed one polymer chain and rotated the other one around its axis from 0° to 360°; thus, all of the possible backbone-nonparallel models were included. We rotated the two polymer chains around their axis at the same time; thus, all of the possible backbone-parallel models were included. The packing energies were calculated every 5° with crystal orbital method at B3LYP/3-21G level; the results showed that model **9** is energetically favorable on the potential surface (the 0° point). We optimized the relative position of the two polymer chains of model **10** along the polymer axis (*z* axis in crystal) and the direction perpendicular to the plane, which contains these two polymers; a slightly more stable structure was located, but the 2_1 helix, which possibly exists in the 2D and 3D structures, was lost and the stability of the 3D structure using these parameters decreased.

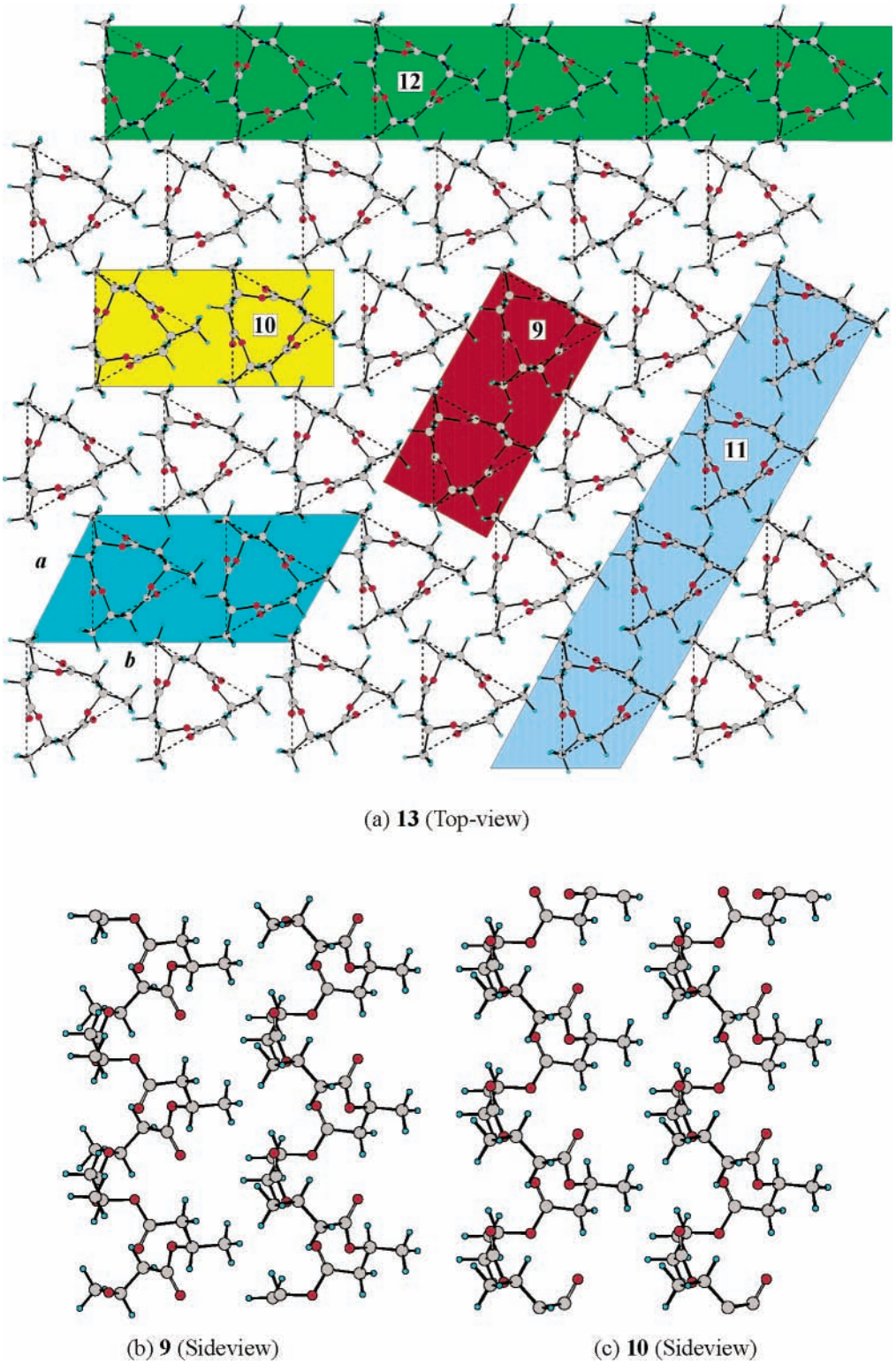

Figure 5. Top view (a) of 3D crystal model **13** constructed by 3_1-helix. Models **9** and **10** are parallel and antiparallel double helices; models **11** and **12** are parallel and antiparallel slabs. **a** and **b** are translational vectors. Panel b shows a side view of model **9**. Panel c shows a side view of model **10**. The carbonyl groups have no strong interaction in these two models.

Results and Discussion

A. Conformation Search. Eighteen conformational minima are located for the diester model **1** (Figure 1). The calculated dipole moments, backbone dihedral angles, entropies, relative enthalpies in the gas phase, relative entropies, and free energies (298 K) in methanol solution are given in Table 1. The data show that this diester structure is very flexible. The relative Gibbs free energies of the 10 most stable conformations are within 1.0 kcal/mol both, in the gas phase and in methanol solution. This result is consistent with the results of NMR studies and MD simulations, which indicate that this polymer is very flexible and has no predominant conformation in solution.[7,12] The torsion angles of **B** and **C** are close to those obtained from experiment (Table 1).

Among the top 10 most stable conformers, six of them have a gauche dihedral angle about the central C−C bond (τ_3), while

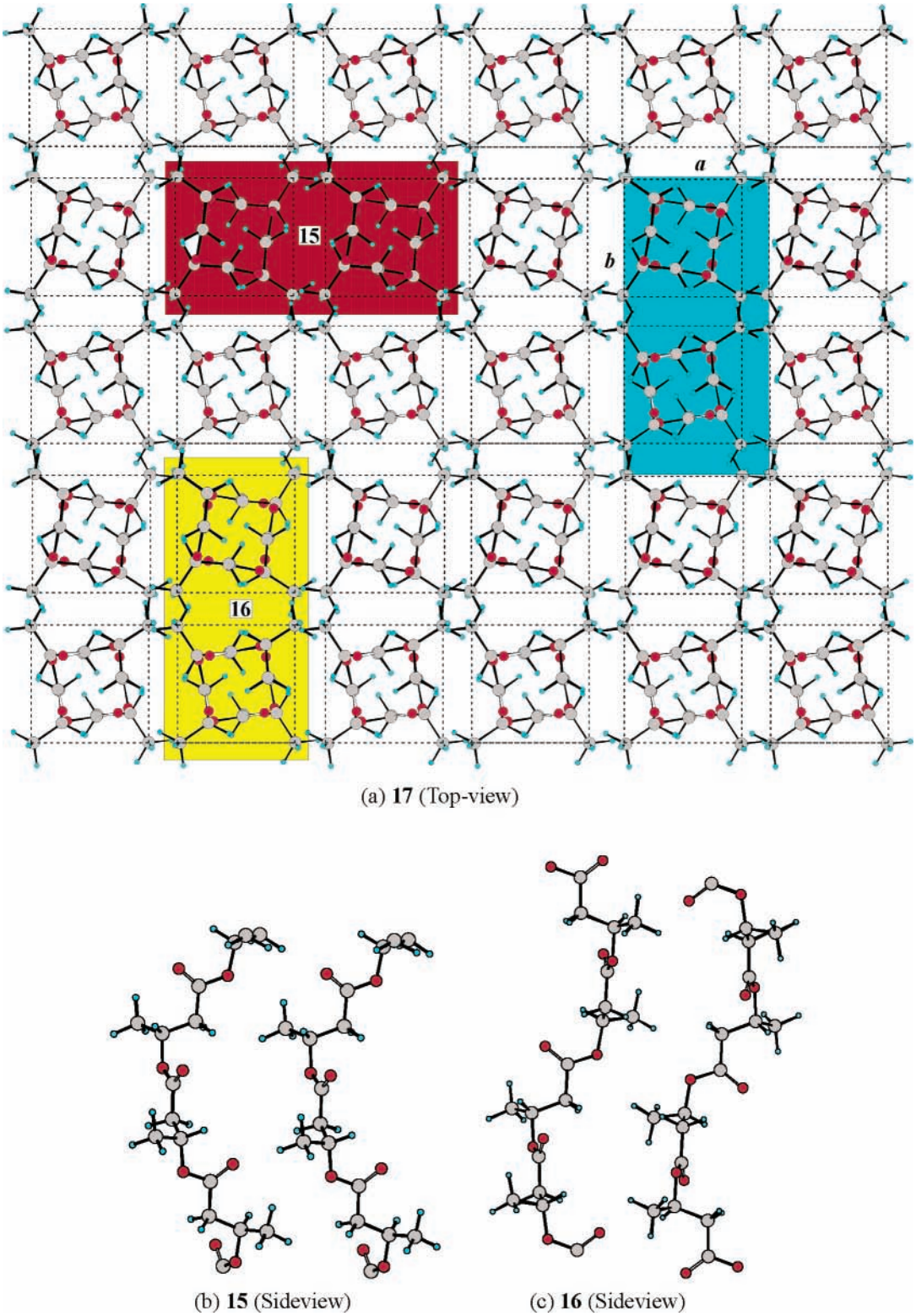

Figure 6. Top view of 3D crystal model **17** constructed by 4_1-helix. Models **15** and **16** are parallel and antiparallel double helices. **a** and **b** are translational vectors. Panel b shows a side view of model **15**. Panel c shows a side view of model **16**. The carbonyl groups have no strong interactions in these two models.

the other four have an anti τ_3 dihedral angle. Those conformers with an anti τ_3 are generally less stable enthalpically but are stabilized by relatively larger entropy. This favorable enthaplic preference for gauche τ_3 originates from an attractive electrostatic interaction between the negatively charged ester oxygen and the positively charged carbonyl carbon. A similar feature has been observed for β-peptides and is partially responsible for the easy formation of helical secondary structures.[10a]

The conformational feature of the diester model is thus very different from those of diamide models of β-amino acids and amyloxy acids,[10a,11c] which strongly favor hydrogen-bonded C6 or C8 conformations ot both. It is thus the lack of hydrogen-bond formation that results in the flexibility of the diester model.

B. Stability and Cooperativity of One Dimension PHB in the Gas Phase. The stable conformers **1B**, **1C,** and **1D** correspond to the basic structural units for the formation of 3_1-,

TABLE 1: Calculated Dipole Moments (D), Torsional Angles (deg), Entropies (cal/(mol·K)), Relative Enthalpies (kcal/mol) in the Gas Phase, and Relative Enthalpies and Free Energies (kcal/mol, 298 K) in Methanol Solution (SCIPCM, $\epsilon = 32.63$) for the Conformers of Diester Model 1[a]

	gas phase								sol SCIPCM model	
conformer	dipole	τ_1	τ_2	τ_3	τ_4	S	ΔH_{gas}[b,c]	ΔG_{gas}[d]	ΔH_{sol}[e]	ΔG_{sol}[f]
A	0.9	180.0	152.0	−175.2	58.6	120.7	1.2 (1.3)	−0.2	1.5	0.1
B	3.3	−174.7	152.5	−65.7	156.6	116.1	0.0 (0.0)	0.0	0.0	0.0
		−176.9[g]	142.2[g]	−62.3[g]	150.7[g]					
C	0.4	−179.4	153.0	−59.7	−47.8	116.8	0.3 (0.6)	0.1	0.2	0.0
		−175[h]	152[h]	−52[h]	−42[h]					
D	2.4	177.7	81.7	−172.9	−175.2	116.9	0.4 (0.1)	0.2	1.1	0.9
E	1.7	178.7	82.9	179.6	44.9	118.0	0.8 (1.2)	0.3	1.1	0.5
F	1.7	−175.2	95.6	−64.4	−81.6	113.0	−0.5 (0.6)	0.4	0.4	1.3
G	1.4	−177.8	80.4	54.7	−103.7	114.6	0.1 (1.0)	0.5	0.5	1.0
H	3.4	180.0	152.7	−168	−173.8	116.7	0.8 (0.3)	0.6	1.2	1.0
I	3.0	−174.0	76.2	49.0	89.2	114.2	0.2 (0.6)	0.7	0.9	1.5
J	3.0	−178.2	95.6	−75.1	90.0	114.4	0.3 (1.2)	0.8	0.6	1.1
K	2.5	178.9	147.5	56.9	−121.3	116.5	1.4 (1.5)	1.3	1.7	1.6
L	2.2	179.7	145.3	51.6	70.8	117.2	2.0 (2.3)	1.7	2.1	1.8
M	0.6	−178.8	−65.7	−64.3	140.8	116.5	2.7 (2.7)	2.5	3.1	3.0
N	1.3	−177.2	−63.3	−158.5	−174.4	115.9	2.4 (2.2)	2.5	3.4	3.5
O	3.1	173.1	−63.7	−52.1	−76.8	114.2	2.1 (2.9)	2.6	2.8	3.4
P	3.4	−178.2	47.0	−165.7	−64.0	116.9	3.6 (3.8)	3.3	4.0	3.7
Q	2.7	−178.3	−73.3	81.8	−112.0	114.8	3.5 (4.6)	3.9	4.7	5.1
R	2.0	177.0	−78.9	65.5	76.7	112.9	4.0 (5.2)	4.9	4.6	5.6

[a] Geometries were optimized at the B3LYP/6-311G* level. [b] MP2/6-311G* single-point energy plus thermal energy correction. [c] The values in parentheses are calculated by B3LYP/6-311G* method. [d] Free energy based on ΔH and ΔS in the gas phase. [e] MP2/6-311G* single-point energy plus solvent effect and thermal energy correction ($\Delta H = \Delta H_{MP2/gas} + \Delta(E_{HF/sol} - E_{HF/gas})$). [f] Free energy based on ΔH in solution and ΔS in the gas phase. [g] Taken from ref 12. [h] Taken from ref 5b.

TABLE 2: Relative Residue Energies (kcal/mol) of Polymers A, B, C, D, and H Derived by Repeating Unit Approach Calculation with the B3LYP/6-311G* and MP2/6-311G* (in Parentheses) Methods and Backbone Dihedral Angles (deg)

	relative energy							torsional angles			
	$n = 2$	$n = 3$	$n = 4$	$n = 5$	$n = 6$	$n = 7$	$n = 8$	τ_1	τ_2	τ_3	τ_4
A	0.65 (1.20)	0.66 (1.23)	0.67 (1.24)	0.65 (1.24)	0.69	0.69	0.70	180	151.7	−174.7	60.0
B	−1.08 (−1.49)	−1.06 (−2.04)	−1.17 (−2.17)	−1.25 (−2.24)	−1.27	−1.30	−1.32	−172.1	154.1	−55.2	128.1
C	0.00 (0.00)	0.00 (0.00)	0.00 (0.00)	0.00 (0.00)	0.00	0.00	0.00	179.7	150.3	−61.2	−54.2
D	−0.58 (0.55)	−0.60 (0.57)	−0.59 (0.59)	−0.60 (0.58)	−0.58	−0.57	−0.55	179.6	80.8	−171.7	176.2
H	−0.21 (1.09)	−0.24 (1.11)	−0.24 (1.11)	−0.24 (1.11)	−0.23	−0.22	−0.20	−179.3	150.9	−168.9	−176.5

2_1-, and 4_1-helices, respectively. The backbone conformations of **1A** and **1H** have been found in the X-ray crystal structure of an octalactone by Bachmann and Seebach.[19] The secondary structures constructed on the basis of these five conformations are denoted as polymer **A**, **B**, **C**, **D**, and **H**, respectively. To understand the relative stabilities of these secondary structures, it would be helpful to understand whether there is cooperative interaction in these structures. Toward this purpose, these structures have been studied with a repeating unit method using a hexaester model Ac−(CHMe−CH_2−CO)$_5$−OCH_2CH_3. The calculated backbone dihedral angles of the repeating units and the residue energies [$E(n) = E_n - E_{n-1}$, $n = 2-8$, where E_n is the total energy of the oligoester with n repeating units] are given in Table 2. Except for polymer **B**, these structures each have constant residue energy, indicating that there is no cooperative interaction in these structures. This is not difficult to understand because the carbonyl dipoles in these structures are not aligned in the same direction. Polymer **B** has been found to possess a small cooperativity because the carbonyl groups form a dihedral angle of about 32.8° with the helix axis. The calculated residue energy for the fifth residue is about 0.2 and 0.8 kcal/mol more stable than the second residue with the B3LYP/6-311G* and MP2/6-311G* methods, respectively. It is also noted that the calculated backbone dihedral angles ($\tau_1-\tau_4$) in polymer **A**, **C**, **D**, and **H** structures are quite similar to those in the corresponding structures **1A**, **1C**, **1D**, and **1H**, respectively. However, the calculated τ_3 and τ_4 in polymer **B** are quite different from those in structure **1B**. This can be attributed to an attractive interaction between the C═O of the ith ester and the Cα−H of the $i-2$ ester. The O···H distance is about 2.54 Å.[20] This interaction is absent in structure **1B**.

Thus, except for the 3_1-helix, the relative stabilities of the other secondary structures can be roughly estimated on the basis of the calculation results of the diester model **1**. We conclude that because of a cooperativity, the 3_1-helix is the most stable secondary structure in the gas phase while the other structures have similar stabilities. In solution, the cooperativity for the 3_1-helix is also reduced and thus cannot be much more stable than the other structures.

It is noted that the polymer **C** structure derived from the repeating unit method of geometry optimization does not correspond to a perfect 2_1-helix. Instead, each HB unit rotates around the helix axis by about 196°. Thus, to form a perfect 2_1-helix, two units of HB have to rotate back by about 33°. We estimated that the adaptation of a perfect 2_1-helix from the fully optimized structure costs about 0.3 kcal/mol per HB unit. Thus, the perfect 2_1-helix is a high-energy conformation, but the energy penalty can be compensated by better crystal packing, especially between parallel helices, as will be discussed in the next section.

C. Crystal Packing Energy. Two different folding patterns of PHB are often discussed in the literature, a 2_1-helix and a 3_1-helix, but only the structure of the 2_1 helix has been found in crystal structures of PHB by stretch-fiber X-ray diffraction measurements.[5] On the other hand, our above calculations indicate that in the gas phase the 3_1-helix is the most stable

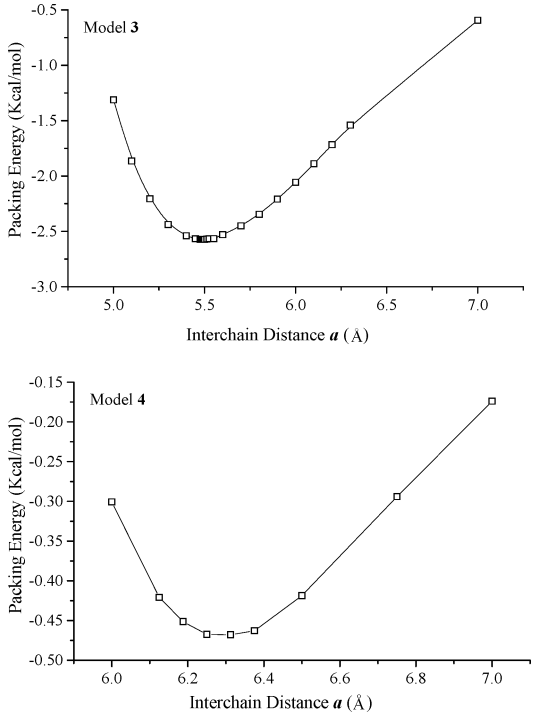

Figure 7. Plot of packing energy as a function of packing distance for parallel double-helix model **3** and antiparallel double-helix model **4**. Energies were calculated with the crystal orbital method at B3LYP/3-21G level.

secondary structure. Then how does one account for the stability of the 2_1-helix in the solid state? To answer this question, crystal packing energies of the 2_1-, 3_1-, and 4_1-helices have been evaluated using the CRYSTAL98 program.[18]

2_1-Helix. As shown in Figure 4, the crystal structure of the PHB features columns of parallel 2_1-helices (vertical). The helices in adjacent columns are antiparallel. Thus, each helix is in direct contact with two parallel helices and four antiparallel helices. The interactions between two parallel helices were studied using model **3**, while the interactions between two antiparallel helices were studied using model **4**. The interaction energy was estimated by stepwise adjustment of the distance between two helices with crystal orbital calculations. Figure 7 shows the location of the best distances for the packings of models **3** and **4**. For model **3**, the best distance of packing is about 5.5 Å, and the calculated packing energy between two parallel 2_1-helices is about −2.6 kcal/mol. For model **4**, the ideal packing distance is increased to about 6.3 Å with a packing energy of only about −0.5 kcal/mol per HB unit. The packing energies of models **5**, **6**, and **7** can be estimated with crystal orbital calculations based on the best structures of models **3** and **4**. The packing energy, E_p, the relative energy, E_R, the unit cell geometrical parameters derived from the crystal orbital calculations, and the density (ρ) of 3D structures are listed in Table 3.

It is interesting that the packing energy of the parallel double-chain model **3** is calculated to be much more stable than the antiparallel double-chain model **4**. Inspection of geometries indicates that the two helices in model **3** involve a translation of about 5.5 Å. The carbonyl groups on the two helices align nearly in a line, head-to-tail, similar to the situation in pleated sheet structures of β-peptides.[10d] Therefore, they have the largest attractive interaction. On the other hand, in the antiparallel model **4**, the carbonyl groups on the two helices do not align in a line anymore. Instead, they align nearly shoulder-to-shoulder and are separated by about 6 Å. Such arrangement does not allow an attractive interaction. Therefore, the small packing energy of −0.5 kcal/mol per HB unit is mainly due to weak van der Waals interactions between the two helices.

TABLE 3: Crystal Packing Energy, E_p, Relative Energy, E_R, the Optimized Unit Cell Parameters in the Crystal Orbital Calculation, and the Density (ρ) of 3D Structures of Models 3−16[a]

model	E_p (kcal/mol)	E_R (kcal/mol)	symm	tosion angles (deg)		unit cell parameters in the calculation and the calculated density	
			2_1-helix				
3	−2.6	−2.6	$P2_111$	τ_1	−176.9	a (Å)	5.4875 (5.76[b])
4	−0.5	−0.5	$P2_111$	τ_2	156.1	b (Å)	12.625 (13.20[b])
5	−5.3	−5.3	$P2_111$	τ_3	−59.1	c (Å)	6.124 (5.96[b])
6	−0.8	−0.8	$P2_111$	τ_4	−36.4	α (deg)	90.0
7	−6.3	−6.3	$P2_12_12_1$			β (deg)	90.0
						γ (deg)	90.0
						ρ (g/cm^3)	1.347 (1.25[c])
			3_1-helix				
9	−0.4	−2.6	$P1$	τ_1	−173.8	a (Å)	8.125
10	−0.3	−2.5	$P1$	τ_2	134.7	b (Å)	15.9
11	−0.8	−3.1	$P1$	τ_3	−58.3	c (Å)	6.258
12	−0.8	−3.0	$P2_111$	τ_4	153.1	α (deg)	90.0
13	−2.5	−4.7	$P3_12_11$			β (deg)	90.0
						γ (deg)	120.73
						ρ (g/cm^3)	0.912
			4_1-helix				
15	−0.9	−2.7	$P2_1$	τ_1	180.0	a (Å)	6.375
16	−0.6	−2.4	$P211$	τ_2	80.6	b (Å)	12.818
17	−3.0	−4.8	$P4_12_12$	τ_3	−172.2	c (Å)	15.711
				τ_4	−173.9	α (deg)	90.0
						β (deg)	90.0
						γ (deg)	90.0
						ρ (g/cm^3)	0.891

[a] For each HB unit of 2_1-helix, 3_1-helix, and 4_1-helix, the zero energy is −304.676 50, −304.672 94 and −304.675 83 au, respectively (at B3LYP/3-21G level using crystal orbital method). [b] Taken from ref 5b. [c] Taken from ref 1c.

In terms of the packing energies of parallel and antiparallel slab models **5** and **6**, the calculated stabilizations are about twice the values of models **3** and **4**, respectively. This indicates that each helix has interactions mainly with two immediate adjacent helices, and its interactions with more remote helices are very small (0.15 kcal/mol additional stabilization for the parallel slab and 0.16 kcal/mol destabilization for the antiparallel slab). The calculated total packing energy of the crystal structure model **7** is about −6.3 kcal/mol. This packing energy is somewhat (0.6 kcal/mol) smaller than the sum of the packing energy of model **5** and twice the packing energy of model **6**, indicating that long-range interactions are slightly destabilizing overall.

In the optimized structure, the translational distance c of model **2** is 6.124 Å; this result is close to the experimental data well (5.96 Å).[5b] From models **3** and **4**, we got $a = 5.4875$ and $b = 12.625$ Å; they are close to the experimental values of 5.76 and 13.20 Å, respectively.[5b]

The calculation result that the parallel slabs provide much of the packing energy for the 2_1-helix crystal is in agreement with experimental observations. Barham et al.[21] have shown that the predominant chain folding in PHB crystal is along the long axis of the single crystal, which is the *a*-axis in Figure 4. When the single crystal was stretched in the direction of the long axis, periodic cracks intersected the long axis; when it is stretched in the direction perpendicular to its long axis, the single crystal can be split into small crystals along the long axis. Thus, both

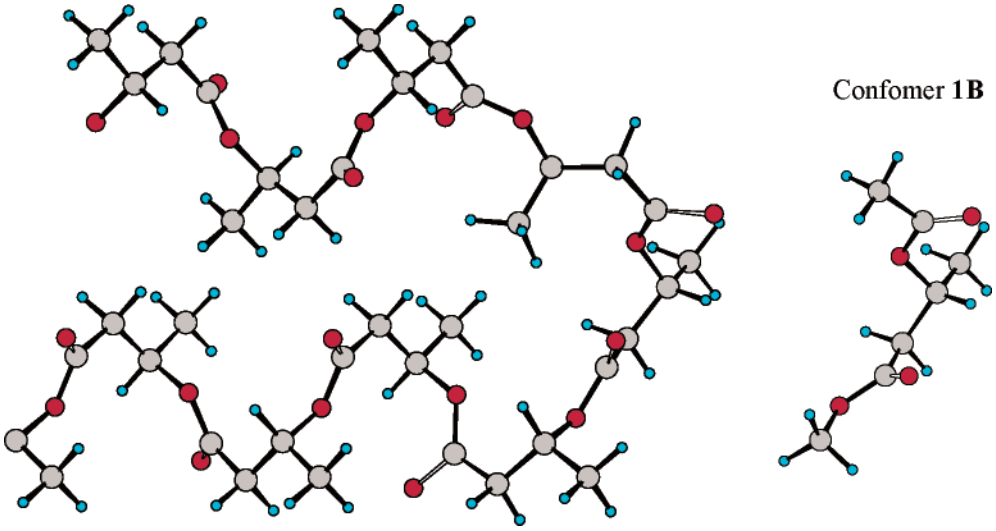

Figure 8. The hairpin structure formed by two antiparallel 2_1-helices and one basic unit of 3_1-helix (**1B**).

experiment and our results suggest that every polymer running across the crystal by successive folds staggering within two parallel slabs, that is, every two neighboring parallel slabs, is formed by the same single polymer.

3_1-Helix. Because there is no structural information available for possible crystal packing consisting of 3_1-helices, we had to make a guess of the packing pattern. This was achieved by doing testing calculations with parallel and antiparallel double helices, models **9** and **10**. Several orientations between the two helices were calculated, and the orientation with the favorable packing energy and symmetry was used to build a crystal-packing pattern. Detailed calculation procedures and results are given in Supporting Information. As shown in Figure 5, each row consisted of alternating antiparallel helices. Thus, parallel and antiparallel double-helix models are **9** and **10**, respectively, and parallel and antiparallel slabs are **11** and **12**, respectively. Each helix is in direct contact with four antiparallel helices and two parallel helices.

The 3-fold 3_1-helix is fatter than the 2_1-helix. Therefore, the ideal packing distance between two parallel helices and antiparallel helices are about 8.1 and 8.0 Å, respectively, considerably larger than those between two 2_1-helices. In addition, the carbonyl groups in the 3_1-helix align about 32° with respect to the helix axis; the dipole−dipole interaction involving two parallel or antiparallel helices is small. The calculations give packing energies of −0.4 and −0.3 kcal/mol for each HB unit in the models **9** and **10**, respectively. The packing energy of each HB unit in parallel slab (**11**) and antiparallel slab (**12**) is about 0.8 kcal/mol. The total packing energy of each HB in model **13** is calculated to be about −2.5 kcal/mol, much smaller than the 6.3 kcal/mol stabilization for the 2_1-helix crystal model **7**.

4_1-Helix. Our model for the 4_1-helix crystal structure was developed in a similar way as that for the 3_1-helix. As shown in Figure 6, each helix has direct contact with four helices, two parallel and two antiparallel. Parallel and antiparallel double-helix models are **15** and **16**, respectively. The parallel double-helix packing brings a stabilization of 0.9 kcal/mol for each HB unit, while each HB unit gains a stabilization of about 0.6 kcal/mol in the antiparallel double-helix packing. The estimated total packing energy for each HB unit in the 3D model **17** is about −3.0 kcal/mol, nearly twice of the sum of models **15** and **16**.

D. Overall Stability. As summarized in Table 3, our model calculations indicate that the 2_1-helix 3D model **7** has a much larger packing energy for each HB unit than the 3_1-helix and 4_1-helix models **13** and **17**. Although each HB unit in the 2_1-helix is calculated to be less stable than that in the 3_1-helix and 4_1-helix by about 2.2 and 1.8 kcal/mol, respectively, the crystal model **7** is still more stable than the crystal models **13** and **17**. From calculated crystal unit cell parameters, it is clear that the 2_1-helix crystal model **7** is much more closely packed than the crystal models for the 3_1-helix and 4_1-helix (**13** and **17**). The calculated density of the model **7** is 1.347 g/cm^3. The experimental value[1c] is about 1.25 g/cm^3. Because the geometrical optimizations were only carried out with models **3** and **4**, the agreement is quite satisfactory.

E. The Structure of the Turn. PHB crystals have a lamellar morphology, the polymer chains running perpendicular to the lamellar crystal surface and doubling back on themselves and crossing the crystal several times.[1c] A controlled degradation experiment of single PHB crystals indicated that PHB is present in a hairpin arrangement and the turn cannot contain more than one or two HB units.[1c] Here, we find that conformer **1B** can function as an ideal turn structure connecting two antiparallel 2_1-helices as shown in Figure 8. Conformer **1B** is a stable conformation for a single HB unit, and the connection should cause little strain because only a small geometrical adjustment is needed.

Summary

A theoretical study on PHB using quantum mechanics methods has been carried out. Conformational search on a diester model **1** reveals that there are 10 conformations within 1.0 kcal/mol of the global minimum, indicating that the backbone of PHB is very flexible. Five interesting secondary structures based on five stable diester conformers have been studied by a repeating unit approach. Only the 3_1-helix is found to possess a weak cooperativity. An ab initio crystal orbital study has been carried out on the 2_1-helix $P2_12_12_1$ crystal and possible crystal models of 3_1-helix and 4_1-helix. The results show that the 2_1-helix crystal has a much stronger packing energy than the other two crystal structures (if they are formed). The strong packing for the 2_1-helix crystal is due to strong dipole−dipole interactions between parallel polymer chains but not due to antiparallel polymer chains. This suggests that the often-suggested antiparallel 2_1-helix bundle for the ion channel may not possess much stabilization.

Acknowledgment. We thank Professor D. Seebach of ETH for directing our attention to this interesting subject.

Supporting Information Available: Calculated total energies and geometrical coordinates of structures **1A**−**R**; detailed procedures for the derivation of crystal structure models of 3_1- and 4_1-helices. This material is available free of charge via the Internet at http://pubs.acs.org.

References and Notes

(1) (a) Doi, Y. *Microbial Polyesters*; VCH: New York, 1990. (b) Müller, H.-M.; Seebach, D. *Angew. Chem., Int. Ed. Engl.* **1993**, *32*, 477. (c) Seebach, D.; Brunner, A.; Bachmann, B. M.; Hoffmann, T.; Kühnle, F. N. M.; Lengweiler, U. D. *Ernst Schering Res. Found. Workshop* **1995**, *28*. (d) Seebach, D.; Fritz, M. G. *Int. J. Biol. Macromol.* **1999**, *25*, 217. (e) Sudesh, K.; Abe, H.; Doi, Y. *Prog. Polym. Sci.* **2000**, *25* 1503.

(2) (a) Brandl, H.; Gross, R. A.; Lenz, R. W.; Fuller, R. C. *Adv. Biochem. Eng. Biotechnol.* **1990**, *41*, 77. (b) Mochizuki, M.; Hirami, M. *Polym. Adv. Technol.* **1997**, *8*, 203. (c) Amass, W.; Amass, A.; Tighe, B. *Polym. Int.* **1998**, *47*, 89. (d) Lee, S. Y.; Lee Y.; Wang, F. *Biotechnol. Bioeng.* **1999**, *65*, 363. (e) Sudesh, K.; Doi, Y. *Polym. Adv. Technol.* **2000**, *11*, 865.

(3) (a) Reusch, R. N.; Sadoff, H. L. *Proc. Natl. Acad. Sci. U.S.A.* **1988**, *85*, 4176. (b) Reusch, R. N.; Huang, R.; Bramble, L. L. *Biophys. J.* **1995**, *69*, 754. (c) Huang, R.; Reusch, R. N. *J. Bacteriol.* **1995**, *177*, 486. (d) Castuma, C. E.; Huang, R.; Kornberg, A.; Reusch, R. N. *J. Biol. Chem.* **1995**, *270*, 12980. (e) Das, S.; Lengweiler, U. D.; Seebach, D.; Reusch, R. N. *Proc. Natl. Acad. Sci. U.S.A.* **1997**, *94*, 9075. (f) Das, S.; Kurcok, P.; Jedlinski, Z.; Reusch, R. N. *Macromolecules* **1999**, *32*, 8781. (g) Resuch, R. N. *Biochemistry* **1999**, *38*, 15666. (h) Reusch, R. N. *Biochemistry (Moscow)* **2000**, *65*, 280. (i) Das, S.; Reusch, R. N. *Biochemistry* **2001**, *40* 2075. (j) Das, S.; Seebach, D.; Reusch, R. N. *Biochemistry* **2002**, *41*, 5307.

(4) (a) Seebach, D.; Burger, H. M.; Müller, H. M.; Lengweiler, U. D.; Beck, A. K. *Helv. Chim. Acta* **1994**, *77*, 1099. (b) Seebach, D.; Brunner, A.; Burger, H. M.; Reusch, R. N.; Bramble, L. L. *Helv. Chim. Acta* **1996**, *79*, 507. (c) Fritz, M. G.; Walde, P.; Seebach, D. *Macromolecules* **1999**, *32*, 574.

(5) (a) Cornibert, J.; Machessault, R. H. *J. Mol. Biol.* **1972**, *71*, 735. (b) Yokouchi, M.; Chatani, Y.; Tadokoro, H.; Tani, H.; Teranishi, K. *Polymer* **1973**, *14*, 267. (c) Cornibert, J.; Marchessault, R. H. *Macromolecules* **1975**, *8*, 296. (d) Brüchner, S.; Meille, S. V.; Malpezzi, L.; Cesàro, A.; Navarini, L.; Tombolini, R. *Macromolecules* **1988**, *21*, 967. (e) Pazur, R. J.; Hocking, P. J.; Raymond, S.; Marchessault, R. H. *Macromolecules* **1998**, *31*, 6585. (f) Seebach, D.; Bürger, H. M.; Müller, H.-M.; Lengweiler, U. D.; Beck, A. K.; Sykes, K. E.; Parker, P. A.; Barham, P. J. *Helv. Chim. Acta* **1994**, *77*, 1099. (g) Sykes, K. E.; McMaster, T. J.; Miles, M. J.; Parker, P. A.; Barham, P. J.; Seebach, D.; Müller, H.-M.; Lengweiler, U. D. *J. Mater. Sci.* **1995**, *30*, 623.

(6) (a) Plattner, D. A.; Brunner, A.; Dobler, M.; Müller, H.-M.; Petter, W.; Zbinden, P.; Seebach, D. *Helv. Chim. Acta* **1993**, *76*, 2581. (b) Seebach, D.; Hoffmann, T.; Kühnle, F. N. M.; Lengweiler, U. D. *Helv. Chim. Acta* **1994**, *77*, 2007.

(7) (a) Kamiya, N.; Inoue, Y.; Yamamoto, Y.; Chujo, R.; Doi, Y. *Macromolecules* **1990**, *23*, 1313. (b) Li, J.; Uzawa, J.; Doi, Y. *Bull. Chem. Soc. Jpn.* **1998**, *71*, 1683. (c) Seebach, D.; Rueping, M.; Waser, P.; Duchardt, E.; Schwalbe, H. *Helv. Chim. Acta* **2001**, *84*, 1821. (d) Albert, M.; Seebach, D.; Duchardt, E.; Schwalbe; H. *Helv. Chim. Acta* **2002**, *85*, 633.

(8) Rueping, M.; Dietrich, A.; Buschmann, T.; Fritz, M. G.; Sauer, M.; Seebach, D. *Macromolecules* **2001**, *34*, 7042.

(9) (a) Seebach, D.; Matthews, J. L. *Chem. Commum*. **1997**, 2015. (b) Gellman, S. H. *Acc. Chem. Res.* **1998**, *31*, 173. (c) Gademann, K.; Hintermann, T.; Schreiber, J. V. *Curr. Med. Chem.* **1999**, *6*, 905. (d) deGrado, W. F.; Hamuro, Y. *J. Peptide Res.* **1999**, *54*, 206. Cheng, R. P.; Gellman, S. H.; DeGrado, W. F. *Chem. Rev.* **2001**, *101*, 3219−3232. (e) Yang, D.; Ng, F.-F.; Li, Z.-J.; Wu, Y.-D.; Chan, W. K.; Wang, D.-P. *J. Am. Chem. Soc.* **1996**, *118*, 9794. (f) Yang, D.; Li, B.; Ng, F.-F.; Yan, Y.-L.; Qu, J.; Wu, Y.-D. *J. Org. Chem.* **2001**, *66*, 7303.

(10) (a) Wu, Y.-D.; Wang, D.-P. *J. Am. Chem. Soc.* **1998**, *120*, 13485. (b) Wu, Y.-D.; Wang, D.-P. *J. Am. Chem. Soc*. **1999**, *121*, 9352. (c) Wu, Y.-D.; Wang, D.-P. *J. Chin. Chem. Soc.* **2000**, *47*, 129. (d) Wu, Y.-D.; Lin, J.-Q.; Zhao, Y.-L. *Helv. Chim. Acta* **2002**, *85*, 3144. (e) Lin, J.-Q.; Luo, S.-W.; Wu, Y.-D. *J. Comput. Chem.* **2002**, *23*, 1551. (f) Mohle, K.; Thormann, M.; Sewald, N.; Hofmann, H.-J. *Biopolymers* **1999**, *50*, 167. (g) Günther, R.; Hofmann, H.-J.; Kuczera, K. *J. Phys. Chem. B* **2001**, *105*, 5559. (h) Damm, W.; van Gunsteren, W. E. *J. Comput. Chem*. **2000**, *21*, 774. (i) Daura, X.; van Gunsteren, W. F.; Mark, A. E. *Proteins* **1999**, *34*, 269. (j) Daura, X.; Jaun, B.; Seebach, D.; van Gunsteren, W. F.; Mark, A. E. *J. Mol. Biol*. **1998**, *280*, 925. (k) Daura, X.; van Gunsteren, W. F.; Rigo, D.; Jaun, B.; Seebach, D. *Chem.*−*Eur. J*. **1997**, *3*, 1410. (l) Daura, X.; Gademann, K.; Schäfer, H.; Jaun, B.; Seebach, D.; Van Gunsteren, W. F. *J. Am. Chem. Soc*. **2001**, *123*, 2393.

(11) (a) Yang, D.; Qu, J.; Li, B.; Ng, F.-F.; Cheung, K.-K.; Wang, D.-P.; Wu, Y.-D. *J. Am. Chem. Soc.* **1999**, *121*, 589. (b) Wu, Y.-D.; Wang, D.-P.; Kyle, W. K. C.; Yang, D. *J. Am. Chem. Soc.* **1999**, *121*, 11189.

(12) Gee, P. J.; Hamprecht, F. A.; Schuler, L. D.; Gunsteren, W. F. V.; Duchartd, E.; Schwalbe, H.; Albert, M.; Seebach, D. *Helv. Chim. Acta* **2002**, *85*, 618.

(13) (a) Becke, A. D. *J. Chem. Phys*. **1993**, *98*, 5648. (b) Lee, C.; Yang, W.; Parr, R. G. *Phys. Rev. B* **1988**, *37*, 785.

(14) Frisch, M. J.; Trucks, G. W.; Schlegel, H. B.; Scuseria, G. E.; Robb, M. A.; Cheeseman, J. R.; Zakrzewski, V. G.; Montgomery, J. A., Jr.; Stratmann, R. E.; Burant, J. C.; Dapprich, S.; Millam, J. M.; Daniels, A. D.; Kudin, K. N.; Strain, M. C.; Farkas, O.; Tomasi, J.; Barone, V.; Cossi, M.; Cammi, R.; Mennucci, B.; Pomelli, C.; Adamo, C.; Clifford, S.; Ochterski, J.; Petersson, G. A.; Ayala, P. Y.; Cui, Q.; Morokuma, K.; Malick, D. K.; Rabuck, A. D.; Raghavachari, K.; Foresman, J. B.; Cioslowski, J.; Ortiz, J. V.; Stefanov, B. B.; Liu, G.; Liashenko, A.; Piskorz, P.; Komaromi, I.; Gomperts, R.; Martin, R. L.; Fox, D. J.; Keith, T.; Al-Laham, M. A.; Peng, C. Y.; Nanayakkara, A.; Gonzalez, C.; Challacombe, M.; Gill, P. M. W.; Johnson, B. G.; Chen, W.; Wong, M. W.; Andres, J. L.; Head-Gordon, M.; Replogle, E. S.; Pople, J. A. *Gaussian 98*, revision A.1; Gaussian, Inc.: Pittsburgh, PA, 1998.

(15) (a) Wiberg, K. B.; Keith, T. A.; Frisch, M. J.; Murcko, M. *J. Phys. Chem.* **1995**, *99*, 9072. (b) Forseman, J. B.; Keith, T. A.; Wiberg, K. B.; Snoonian, J.; Frisch, M. J. *J. Phys. Chem.* **1996**, *100*, 16098. (c) Tomasi, J.; Bonaccorsi, R. *Croat. Chem. Acta* **1992**, *12*, 69.

(16) Frisch, M. J.; Trucks, G. W.; Schlegel, H. B.; Gill, P. M. W.; Johnson, B. G.; Robb, M. A.; Cheeseman, J. R.; Keith, T.; Petersson, G. A.; Montgomery, J. A.; Raghavachari, K.; Al-Laham, M. A.; Zakrzewski, V. G.; Ortiz, J. V.; Foresman, J. B.; Cioslowski, J.; Stefanov, B. B.; Nanayakkara, A.; Challacombe, M.; Peng, C. Y.; Ayala, P. Y.; Chen, W.; Wong, M. W.; Andres, J. L.; Replogle, E. S.; Gomperts, R.; Martin, R. L.; Fox, D. J.; Binkley, J. S.; Defrees, D. J.; Baker, J.; Stewart, J. P.; Head-Gordon, M.; Gonzalez, C.; Pople, J. A. *Gaussian 94*, revision B.3; Gaussian, Inc.: Pittsburgh, PA, 1995.

(17) (a) Wu, Y.-D.; Zhao, Y.-L. *J. Am. Chem. Soc*. **2001**, *123*, 5313. (b) Zhao, Y.-L.; Wu, Y.-D. *J. Am. Chem. Soc*. **2002**, *124*, 1570.

(18) Saunders, V. R.; Dovesi, R.; Roetti, C.; Causà, M.; Harrison, N. M.; Orlando, R.; Zicovich-Wilson, C. M. *CRYSTAL98 User's Manual*; University of Torino: Torino, Italy, 1998.

(19) Bachmann, B. M.; Seebach, D. *Helv. Chim. Acta* **1998**, *81*, 2340.

(20) (a) Vargas, R.; Zarza, J.; Dixon, D. A.; Hay, B. P. *J. Am. Chem. Soc*. **2000**, *122*, 4750. (b) Kryachko, E. S.; Zeegers-Huyskens, T. *J. Phys. Chem. A* **2001**, *105*, 7118.

(21) Barman, P. J.; Keller, A.; Otun, E. L.; Holmes, P. J. *J. Mater. Sci.* **1984**, *19*, 2781.